Cyclotron resonance in epitaxial $Bi_{1-x}Sb_x$ films grown by molecular-beam epitaxy

J. Heremans, D. L. Partin, and C. M. Thrush
Physics Department, General Motors Research, Warren, Michigan 48090-9055

G. Karczewski, M. S. Richardson, and J. K. Furdyna
Department of Physics, University of Notre Dame, Notre Dame, Indiana 46556
(Received 3 May 1993; revised manuscript received 1 July 1993)

The far-infrared magnetotransmission of thin films of semiconducting and semimetallic $Bi_{1-x}Sb_x$ alloys grown by molecular-beam epitaxy has been measured at fixed photon energies between 2.5 and 21.4 meV in magnetic fields up to 6 T, at $T=1.8$ K. The samples, grown on BaF_2 substrates with composition $0 \le x \le 22.5\%$, were monocrystalline, with the trigonal axis perpendicular to the surface plane. The measurements were carried out in Faraday and Voigt geometries, with the magnetic field oriented parallel to binary, bisectrix, and trigonal axes of the films. Cyclotron-resonance lines of both electrons and holes were observed. From them, we establish the composition dependence of the effective-mass tensor, of the direct L-point band gap, and of the energy overlap in the semimetallic samples. We conclude that all band-structure parameters are the same in the films as in bulk $Bi_{1-x}Sb_x$ alloys, except for the energy overlap, which is increased by 16 meV independently of composition, possibly because of the strain induced by the substrate.

INTRODUCTION

The heavy group-V elements Bi, Sb, and As, are semimetals because there is a small overlap between the bottom of their conduction bands and the top of their valence bands.[1] However, bismuth-antimony alloys, $Bi_{1-x}Sb_x$, with 7 at. % Sb $< x <$ 23 at. % Sb are semiconductors with a very narrow energy gap.[2,3] The nonlinear optical properties of thin $Bi_{1-x}Sb_x$ films rival those of more conventional II-VI compound narrow-gap semiconductors.[4] Historically, bismuth has been among the very first materials on which important effects have been found, most notably the Hall effect, the thermoelectric effects, the Shubnikov–de Haas and de Haas–van Alphen oscillations, and the effect of size quantization.[5] Because of the small direct energy gap at the L point in bismuth and $Bi_{1-x}Sb_x$ alloys, the electrons and light holes have strongly nonparabolic energy dispersion relations, very small effective masses, and very high carrier mobilities. A review of the electronic properties of the group-V semimetals is given by Dresselhaus,[1] and the properties of electrons in bismuth are reviewed by Edel'man.[6]

The coupled electron and "light" hole bands in bismuth near the L point are conveniently described by a simple Lax two-band model.[7] If we define the zero of the energy scale to be in the middle of the band gap, the dispersion relations for the conduction and valence bands near the L points are

$$E(k)=\pm\tfrac{1}{2}[E_G^2+2E_G\hbar^2\mathbf{k}\cdot\alpha\cdot\mathbf{k}/m_0]^{1/2}\ , \tag{1}$$

where α is the inverse of the effective-mass tensor m at the band extrema, and m_0 is the free-electron mass. In the crystallographic axis system,[8] m is given by

$$\alpha^{-1}=m=\begin{bmatrix} m_1 & 0 & 0 \\ 0 & m_2 & m_4 \\ 0 & m_4 & m_3 \end{bmatrix}\ . \tag{2}$$

The dispersion relation of the holes near the T point can be described by a simple parabolic model, in which the holes have effective masses $m_{T1}=m_{T2}$ in any direction perpendicular to the trigonal axis, and m_{T3} along the trigonal axis. Values for the relevant band parameters of bismuth at 4.2 K are summarized in Table I. We note[9] that there is an agreement of better than 3% between the values for the effective Bohr magnetons obtained from the magneto-optical data of Vecchi and Dresselhaus[10] and the values calculated from the effective masses in Dinger and Lawson,[11] and in the seminal reference in the Russian literature, Edel'man and Khaikin.[12] Magneto-optical data on trigonally oriented bismuth were reported by Maltz and Dresselhaus.[13] Subsequent experimental work on the band structure of bismuth is summarized in

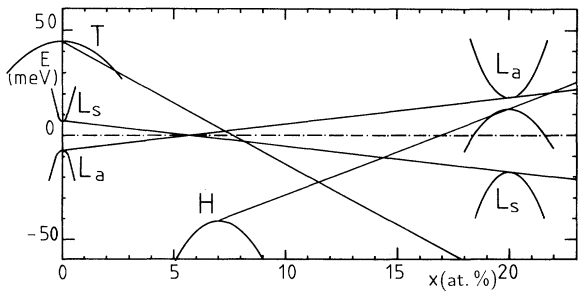

FIG. 1. Energy band structure of $Bi_{1-x}Sb_x$ allows as a function of Sb concentration.

TABLE I. Values for the band parameters of bulk bismuth around 4.2 K.

L-point energy gap	E_g	13.6 meV	Vecchi and Dresselhaus (1974)
Electron and hole density	$n=p$	2.7×10^{17} cm^{-3}	Hartmann (1969)
Electron masses at band edge	m_1	$0.001\,19m_0$	Dinger and Lawson (1973)
	m_2	$0.263m_0$	
	m_3	$0.005\,16m_0$	
	m_4	$0.0274m_0$	
Hole masses	m_{T1}	$0.064m_0$	Dinger and Lawson (1973)
	m_{T2}	$0.064m_0$	
	m_{T3}	$0.69m_0$	
Electron Fermi energy	E_{Fe}	27.2 meV	from n, and effective masses
Hole Fermi energy	E_{Fh}	10.8 meV	from p, and effective masses
Energy overlap	E_o	38 meV	from $E_{Fe}+E_{Fh}$

Ref. 14, and references quoted therein.

Bulk $Bi_{1-x}Sb_x$ alloys can be grown in any proportion, in the $A7$ crystal structure. They undergo two semimetal-to-semiconductor transitions with increasing Sb concentration x. Figure 1, adapted from Ref. 15, but with the T-hole line from Ref. 3, shows diagrammatically the semimetal-to-semiconductor transition which occurs in the concentration range studied here. With increasing x, the L-point direct gap E_G and the energy overlap E_0 first decrease. At $x\simeq5.6$ at.% Sb, the bonding L_s and antibonding L_a bands invert. Around 7 at.% Sb, the T-point band crosses the L_a band, and the material becomes an indirect-gap semiconductor. Above about 8 at.% Sb, the T band crosses the L-point valence band L_s, so that for $8\%<x<15\%$, the material is a direct-gap semiconductor akin to PbTe. The energy diagram for higher Sb concentrations is summarized in Ref. 3. At $x\simeq15\%$, a valence band (at the H point) crosses L_s and the alloys are indirect-gap semiconductors (conduction band at the L point, valence band at the H point). At $x\simeq22\%$, the H band crossses the L-point conduction band, and the alloys become semimetals again, now with a band structure akin to that of Sb.

We report here on the first magneto-optical data taken on epitaxial bismuth and $Bi_{1-x}Sb_x$ films grown by molecular-beam epitaxy (MBE) on insulating BaF_2, and produce the first set of data on the effective masses, direct L-point energy gap, and energy overlap of these films. The concentration range covered in this investigation is $0\le x\le22.5\%$, corresponding to the entire region shown in Fig. 1.

EXPERIMENT

We have grown thin single-crystal Bi films epitaxially on cleaved $\langle111\rangle$ BaF_2 substrates using a Physical Electronics Model 400 molecular-beam epitaxy apparatus.[16–18] The Bi and $Bi_{1-x}Sb_x$ films have their trigonal axes oriented along the direction normal to the substrate plane. The system is load locked, and has an ion-pumped preparation chamber with a base pressure of 10^{-9} Torr in which substrates may be heated before growth. The samples are then transferred to a growth chamber, which is cryopumped to a base pressure of 10^{-10} Torr. BaF_2 substrates are damaged by brief exposures to electron beams, so that it is impossible to use reflection high-energy diffraction (RHEED) to observe the initial stages of nucleation and growth of Bi films. Films grown with substrates held at temperatures of 150° C have microscopically rough surface morphologies. At higher temperatures, no film would nucleate, except near cleavage steps on the BaF_2 surface. Therefore, we nucleated the first 200 Å of the films at 100 °C, and then increased the substrate temperature to a final growth temperature much closer to the melting point. Morelli, Partin, and Heremans[19] describe the growth and galvanomagnetic properties of epitaxial single-crystal films of $Bi_{1-x}Sb_x$ alloys, with $x=1.97\%$, 5.6%, 8.7%, 10.3%, and 12.3%, well into the semiconductor regime, as can be seen from Fig. 1. The samples for the present study come from the same growths, and also include Sb concentrations of $x=14.6\%$, 17.5%, 20.0%, and 22.5%, for which no transport data are available. The MBE growth technique was the same for the $Bi_{1-x}Sb_x$ films as for pure Bi films, with the Sb concentration deduced from the flux during growth and verified by neutron activation analysis on one film. The films were grown at 250 °C, and had a nominal thickness of 1 μm.

The carrier densities of the films with $x\le12.3\%$ are reported in Ref. 19, and are copied here in Table III. The electron densities were not different from the hole densities by more than $\approx2\times10^{16}$ cm^{-3}. The samples with $x>8.7\%$ have electron densities in the 10^{16} cm^{-3} range at low temperatures, and are thus presumably semiconductors. The energy gap of the epitaxial films, calculated from the temperature dependence of the resistivity,[19] appears to open up faster with x than in the bulk alloys.[20] Morelli, Partin, and Heremans[19] point out that the lattice constant of the films along the trigonal axis, as measured by x-ray diffraction, is consistently larger than that of the bulk alloys, and speculate that the compressive strain in the films produces a shift in the edges of the conduction and valence bands.

Far-infrared (FIR) magnetotransmission spectra were recorded at fixed photon wavelengths as a function of a magnetic field, applied parallel to the binary, the bisectrix, and the trigonal axes of each sample. The FIR photon energy range was 2.1–21.4 meV. The propagation direction of the FIR beam was either parallel to the field (Faraday configuration) or perpendicular to the field

(Voigt configuration). In the Faraday configuration, the incident radiation was circularly polarized, and the magnetic field was applied in both polarities, giving spectra in both the cyclotron resonance active (CRA) and inactive (CRI) modes. In the Voigt configuration, two polarizations were examined, one with FIR electric field parallel to the applied dc magnetic field (Voigt parallel configuration), and one with the FIR electric field perpendicular to the direction of the dc magnetic field (Voigt perpendicular). An example of a trace in Faraday configuration is shown in Fig. 2.

Several minima can be observed in the magnetotransmission trace, corresponding to magnetic fields at which the separation between the Landau levels equals the incident FIR photon energy. The locations of these minima can be plotted as the abscissa on a fan chart, which has as ordinate the photon energy. Such charts were generated for all samples in all configurations. In particular, for the sample with $x=8.7\%$ shown in Fig. 2, in the Faraday circularly inactive polarization (CRI), two resonances are clearly distinguished. The low-field resonance observed for $\lambda=229$, 184, 163, 119, 96.5 μm also appears at the same field value in the circular active (CRA) polarization, indicating that it is the tilted orbit cyclotron resonance of electrons located in the three L-point pockets of the conduction band. The high-field transmission minimum observed only in the CRI polarization for $\lambda=229$, 184, and 163 μm can be assigned to holes in the T-point valley.

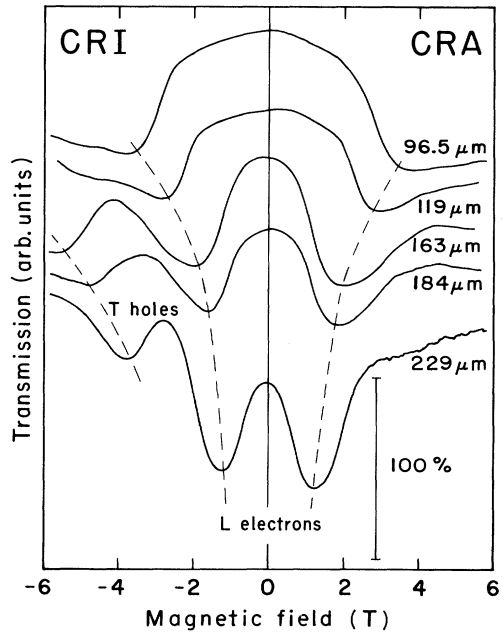

FIG. 2. Magnetotransmission traces of the sample with $x=8.7\%$, as a function of magnetic field at 1.8 K. The wavelengths at which the traces were recorded are indicated. The traces were taken in the Faraday configuration, using circularly polarized FIR waves.

DISCUSSION

The Maltz and Dresselhaus[13] model describes the strongly nonparabolic dispersion of the L-point carriers in $Bi_{1-x}Sb_x$ alloys in the presence of a quantizing magnetic field H. This model assumes that the orbital levels and the spin-split levels are degenerate. We use it to fit all Landau levels of L-point carriers when H is along the trigonal direction, and the higher index Landau levels ($j \geq 1$) when the field is oriented parallel to the binary or bisectrix axes. Electron and light-hole bands are assumed symmetric. In the Maltz and Dresselhaus model, the magnetic energy level index j is related to the orbital and spin quantum numbers n and s by

$$j=n+\tfrac{1}{2}-s\ , \tag{3}$$

where $n=0,1,2,\ldots$ and $s=+\frac{1}{2}$ or $-\frac{1}{2}$. The energy dispersion relations are then

$$E(k)=\pm\{(E_G/2)^2+E_G[\beta Hj+\hbar^2k^2/(2m_H^*)]\}^{1/2}\ , \tag{4}$$

in which the $-$ and $+$ signs correspond to the relation for holes and electrons, respectively. Here K is the wave vector along the magnetic field; m_H^* is the effective mass in that direction, the "longitudinal" effective mass, given by

$$m_H^*=\mathbf{h}\cdot m\cdot\mathbf{h}\ , \tag{5}$$

where m is the effective-mass tensor and $\mathbf{h}$ is the unit vector along the direction of the field; β is the effective Bohr magneton, related to the effective-mass tensor m via

$$\beta=\beta_0[m_H^*/\det(m)]^{1/2}\ , \tag{6}$$

where β_0 is twice the free Bohr magneton,

$$\beta_0=e\hbar/m_0\ , \tag{7}$$

and e and m_0 are the free-electron charge and mass. The effective Bohr magneton is also directly related to the cyclotron mass m_c^*:

$$m_c^*=m_0\beta_0/\beta\ . \tag{8}$$

There is no mechanism in the Maltz and Dresselhaus model by which the band edge of the lowest ($j=0$) level can vary with field. Such variation was observed experimentally when the field is oriented along the binary or bisectrix directions. A more complete model, describing the field dependence of the $j=0$ level when the field is oriented along these directions, is given in Ref. 14, and was used to analyze the results in the present work.

The Fermi surface of the electrons and the light holes consists of three ellipsoidal pockets located at the L points of the Brillouin zone. For fields oriented along the trigonal axis, these three pockets are degenerate, and the Landau levels will be indexed TRI. When the field is applied along the binary axis, two pockets are degenerate, and have a lighter cyclotron mass (indexed LBN, for "light binary") than the pocket which presents its largest cross section to the field (indexed HBN for "heavy binary"). Similarly, for fields along the bisectrix direction, there are two pockets with a "heavy bisectrix" cy-

clotron mass (HBX), and one with a light mass (LBX). The T-point holes are located in a single pocket with rotation symmetry around the trigonal axis, so that they have the same cyclotron mass and Bohr magneton for fields along the bisectrix and binary axes (indexed T1=T2), and a different mass for fields along the trigonal axis (indexed T3).

The fan charts for each sample can be fitted by choosing values for the following parameters: For the L point: E_G, β_{TRI}, β_{LBX}, β_{HBX}, β_{LBN}, and β_{HBN}; for the T point: β_{T1} and β_{T3}. The HBN and T1 lines are not seen in most samples. In semimetallic samples, the energy overlap E_0 is also to be determined from the electron and hole concentrations given in Ref. 19. In the samples with $x \geq 8.7\%$, we observe only the cyclotron-resonance ($j=0$ to $j=1$) line, and the fit is simple. We show the fan charts in Fig. 3 for the sample with $x=14.6\%$, in which the data points are the observed L-point transitions, and the lines represent the fits. Similar results are obtained on all samples with $x \geq 8.7\%$. The values obtained for the magnetons are given in Table II.

Two semimetallic samples in our set, $x=0$ and $x=1.94\%$, showed transitions between several different Landau levels. Since it was difficult to index the transitions *a priori*, we chose to calculate the Landau levels as a function of field, and to represent the observed transitions on those charts. In Fig. 4, we show the different Landau levels calculated for a pure Bi film, following the equations described in the beginning of this section and using the mass tensor elements and E_G values of Ref. 10. The Hall electron (n) and hole (p) densities measured on this film and reported in Ref. 16 are much higher ($n=p \simeq 7.8\times10^{17}$ cm^{-3}) than in bulk Bi ($n=p=2.7\times10^{17}$ cm^{-3}). We assume that this is entirely attributable to an increase of the overlap energy in the film ($E_o=63$ meV) over what it is in the bulk ($E_o=38$ meV). This assumption will be discussed later. The Landau levels of the T-point holes are represented in Fig. 4 as short-dashed lines, starting at an energy of $E_o+E_G/2$ (70 meV) above the middle of the L-point gap. The solid lines in the free frames of the figure are, respectively. the LBN, LBX, and TRI electrons (at positive energies) and L-point holes (at negative energy). The long-dashed lines are the HBN and HBX electrons. The Fermi level (solid line starting near 50 meV) is obtained from the condition that the total density of electrons equals the total density of holes. Given such a Landau-level chart, we can fit the energies and fields that give rise to minima in the magnetotransmission. The selection rule is $\Delta j=\pm1$, and transitions must straddle the Fermi level. The transitions observed in magnetotransmission are shown as vertical lines. They fit the calculated Landau levels rather well, and this strengthens the validity of our assumptions that the L-point gap and effective masses in the Bi films are similar to those of bulk Bi, but that the energy overlap is increased. The results on the film with $x=1.94\%$ will be described later.

We show in Fig. 5 the values of E_G, the direct L-point energy gap, as a function of x, as determined by fits to the cyclotron-resonance lines. E_G is defined here as E_{Ls}-E_{La} for $x<5.5\%$, and as E_{La}-E_{Ls} for $x>6\%$, so that $E_G \geq 0$

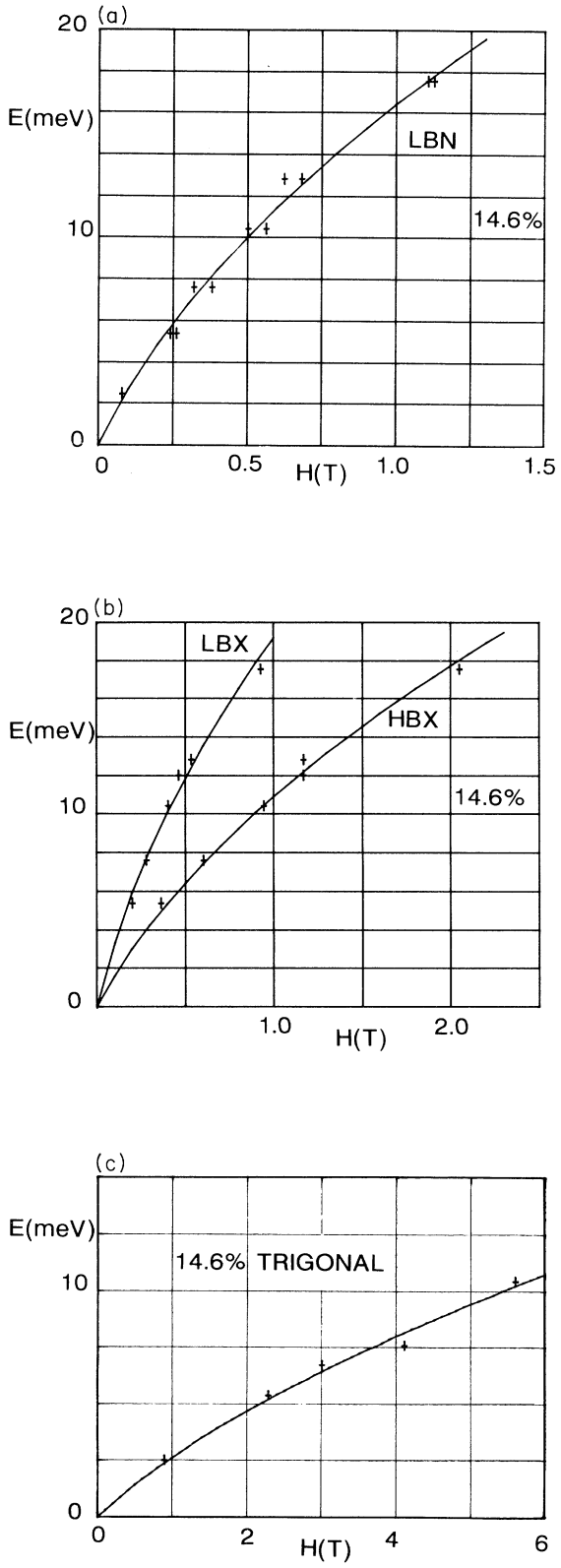

FIG. 3. Fan charts of the sample with $x=14.6\%$. The magnetic field is applied parallel either to the binary (frame LBN), the bisectrix (frames LBX,HBX), or the trigonal (TRIGONAL) directions of the crystals.

TABLE II. Measured energy gaps and effective Bohr magnetons for $Bi_{1-x}Sb_x$ alloys of different x values. The question marks indicate lines observed, but not well identified.

x (at.% Sb)	E_G (meV)	β T holes (T3) (meV/T)	β TRI (meV/T)	β LBX (meV/T)	β HBX (meV/T)	β LBN (meV/T)	β HBN (?) (meV/T)
0	13.6	1.8	9.7	73	44	70	9.1
1.97	8.19	2.1	14.6	135	78	109	
8.70	11.6	1.3	6.5	77	35	59	5.6
10.3	16.3	1.3	5.9	61	26	42	3.0
			15 (?)				
12.30	14.6	1.8	6.3	52	23	42	
			13 (?)				
14.6	18.8	2.0	3.1	39	17	31	
17.5	47	2.3		22	10	18	
20	45					12	
						6.7 (?)	
22.5	36	2.5				16	
						7.2 (?)	

for all x. The straight line corresponds to a fit

$$E_G = |13.6 - 2.44x| \ , \tag{9}$$

where E_G is in meV, and x is in at. % Sb. The behavior is identical to that observed for bulk samples.[15] The accuracy of our fit of E_G to the fan charts is strongly decreased for samples with large x because as the nonparabolicity in the dispersion relation is decreased, so is the curvature in the fan charts, from which E_G is determined. This measurement of $E_G(x)$ gives results that are very similar to the data reported in Ref. 19, where $E_G(x)$ is deduced from the thermally activated behavior of the resistivity. Morelli, Partin, and Heremans[19] point out that their values increase faster with x than those obtained by Jain[20] from the resistivity of bulk samples, and attribute this to the presence of strain in the film. The fact that the present data agree both with the optically determined values of $E_G(x)$ on bulk alloys, and with the transport data on films, suggests that the deviation in the transport data is mostly due to a change in the overlap energy E_o, probably induced by the strain in the films. This again justifies our assumption that the increase in carrier density in pure Bi is entirely due to an increase in E_o.

Plots of the relative change in the effective Bohr magneton β [Eqs. (6)–(8), $\beta \propto 1/m_c^*$] measured on the films are shown in Fig. 6 as a function of antimony content for the LBX, HBX, and LBN electrons. The reference point is the magneton of pure Bi. The ordinate is β_{Bi}/β, which corresponds to the plot of m^*/m^*_{Bi} shown in Ref. 15. $\beta_{Bi}/\beta \geq 0$ for all samples, and equals zero at the crossover point of the L_a and L_s bands. The relative change in β_{Bi}/β with x is surprisingly close to what we expect from earlier bulk alloy data. The lines in Fig. 6 are best fits obtained for the value of m^*/m^*_{Bi} for bulk alloys (x given in at. % Sb):[15]

$$m^* = m^*_{Bi}|(1 - 0.096x^{1.367})| \ . \tag{10}$$

The L-point masses for epitaxial $Bi_{1-x}Sb_x$ films thus vary with x, much as the masses in bulk alloys. All the mass components have the same dependence on x, within the accuracy of our experiment, and change continuously through the band crossing.

It is interesting that we did observe resonances which might be ascribed to HBN electrons. The values labeled HBN given in Table II are deduced from resonances in our spectra which have magnetons of the order of what we would calculate for HBN electrons. These resonances were not expected, because they arise from forbidden cyclotron transitions due to ellipsoids nominally oriented perpendicularly to the magnetic field. It is possible that the weak resonance transitions observed in samples with $x = 0\%$, 8.7%, and 10.3% arise from a small misorientation of the field with respect to the binary axis. The HBN label given to them in Table II is thus only speculative.

Using Eqs. (9) and (10), we calculated the Landau levels for the film with $x = 1.94\%$. To accommodate the Hall density $n = p \simeq 5.8 \times 10^{17}$ cm^{-3},[19] we require an overlap $E_o = 53.5$ meV. The transitions obtained from the magnetotransmission curves were then plotted together with the Landau-level energies versus magnetic field. This served to index the transitions. The effective Bohr magnetons were then fitted, and the results reported in Table II and in Fig. 5.

In order to provide a ready reference, we summarize in Table III the effective-mass tensor components calculated from Eq. (10) for all our samples, and for one additional sample ($x = 5.6\%$) measured in Ref. 19 but not in the present work. The electron and hole densities measured in Ref. 19 are also given, along with the electron and T-point hole Fermi energies that can be calculated from the mass tensor components and the densities. The T-hole masses were assumed to be those of pure Bi (see Table I). The energy overlap E_o can then be calculated for the semimetallic samples as

$$E_o = E_{Fe} + E_{Fh} \tag{11}$$

and is also given in Table III. The origin of the carriers in the samples with $x > 8.7\%$ is unclear. The dependence of E_o on x can then be fitted to

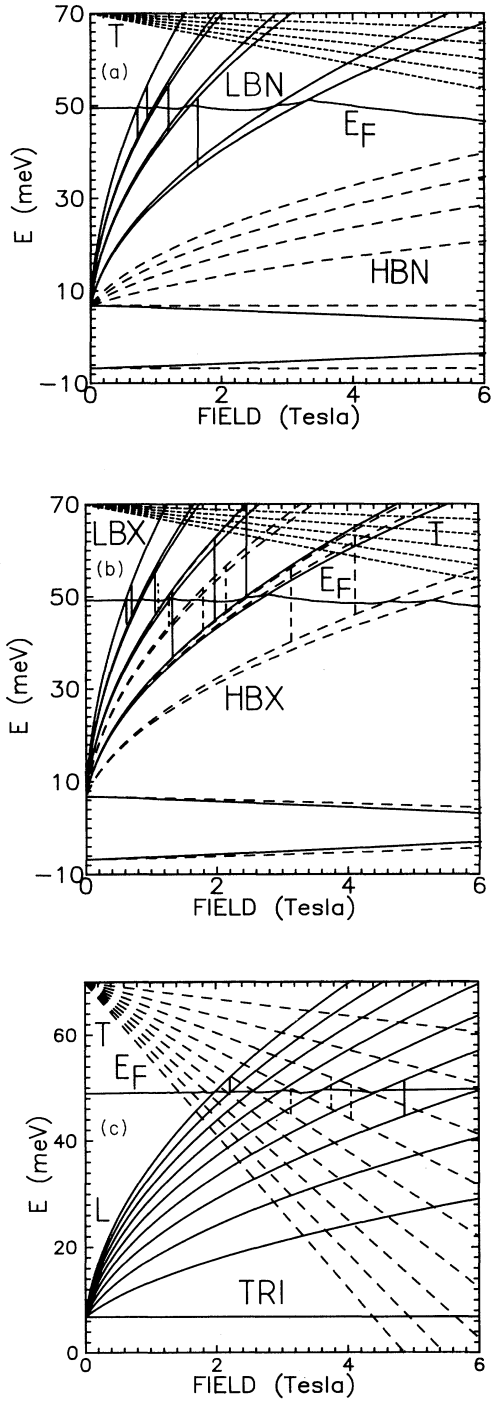

FIG. 4. Landau levels calculated for a pure Bi film in the presence of an applied magnetic field along the binary (LBN,HBN), bisectrix (LBX,HBX), or trigonal (TRI) axes. The Landau levels of the T-point holes are represented as short-dashed lines in the two upper frames, and are indexed T in the lower frame. The solid lines are the LBN, LBX, or TRI electrons (at positive energies) and L-point holes (at negative energies). The long-dashed lines are the HBN or HBX electrons. The Fermi level is the solid line starting at 49 meV. The transitions observed in magnetotransmission are shown as vertical lines (solid lines for LBN and LBX electrons, dashed lines for HBX electrons and T-point holes).

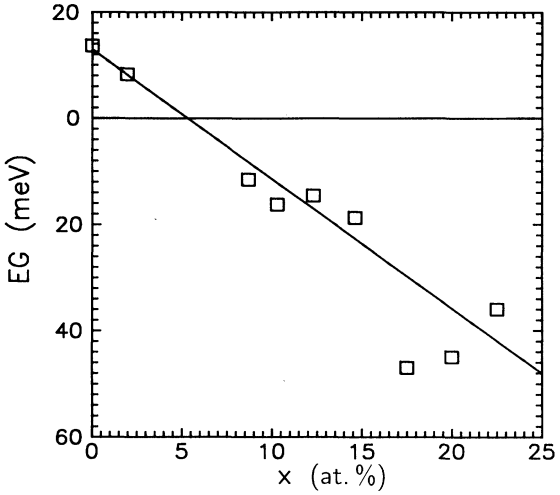

FIG. 5. Direct L-point energy gap E_G as a function of x, as determined by fits to the cyclotron-resonance lines. The straight line corresponds to Eq. (9), which was determined for bulk samples. In the convention used here (see text), $E_G \geq 0$ for all x values.

$$E_o = 63.4 - 6.5x \text{ (meV)}, \tag{12}$$

where x is in at. % Sb. The slope of this regression is very similar to that obtained on bulk alloys[3] [$E_o = 46.9 - 6.013x$ (meV)], but the intercept is 16 meV higher in the films than in bulk alloys. This justifies, *a*

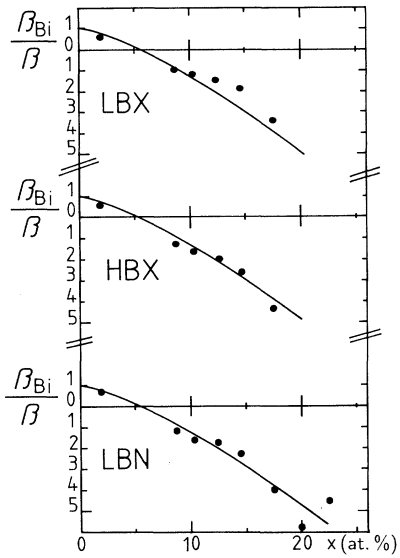

FIG. 6. Relative change in the effective Bohr magnetron, $\beta_{Bi}/\beta = m^*/m^*_{Bi}$, measured on the films as a function of antimony content x, normalized to the magneton of pure Bi. Again, $\beta_{Bi}/\beta \geq 0$ on both sides of the $\beta_{Bi}/\beta = 0$ line, which is crossed when the L_a and L_s bands invert. The solid lines are best fits obtained for the value of m^*/m^*_{Bi} for bulk samples in Ref. 15. The three frames correspond to the Bohr magnetons as fitted for the light bisectrix electrons (LBX), the heavy bisectrix electrons (HBX), and the light binary electrons (LBN).

TABLE III. Summary of electron effective masses, electron and hole densities from Ref. 19, calculated electron and hole Fermi energies, and the energy overlap for semimetallic samples ($x \leq 8.7\%$). No magneto-optical data were obtained on the sample with $x = 5.6\%$, but Morelli, Partin, and Heremans (Ref. 19) report its carrier densities.

x (at.% Sb)	m_1 ($10^{-3}m_0$)	m_2 ($10^{-1}m_0$)	m_3 ($10^{-3}m_0$)	m_4 ($10^{-2}m_0$)	n 10^{17}(cm^{-3})	p 10^{17}(cm^{-3})	E_{Fe} (meV)	E_{Fh} (meV)	E_o (meV)
0	1.19	2.63	5.16	2.74	7.86	7.79	41	21	63
1.97	0.90	2.0	3.9	2.1	5.89	5.79	36	17	53
5.6	0.014	0.031	0.060	0.032	1.48	1.64	19	7.3	26
8.7	1.0	2.2	4.4	2.3	0.20	0	7	≤ 0	≤ 7
10.3	1.6	3.5	6.8	3.6	0.61	0.41	11		
12.3	2.3	5.2	10	5.4	0.48	0.38	8		
14.6	3.3	7.2	14	7.5					
17.5	4.5	10	20	10					
20	5.6	12	25	13					
22.5	6.9	15	30	16					

posteriori, the hypothesis made about the band overlap in this work, and is consistent with the results of Morelli, Partin, and Heremans,[19] which were based on the temperature dependence of the resistivity.

SUMMARY

The cyclotron-resonance data on epitaxial $Bi_{1-x}Sb_x$ films, with $0 \leq x \leq 22.5\%$, grown by MBE on (111) BaF_2 substrates can be explained using the known band-structure parameters of bulk $Bi_{1-x}Sb_x$ alloys. Only the overlap energy E_0 between the L-point conduction band and the T-point valence band differs by about 16 meV between the films and bulk crystals, possibly because of the influence of strain induced by the lattice mismatch between film and substrate.

ACKNOWLEDGMENT

The work at Notre Dame was supported by NSF Grant No. DMR 9208400.

[1]M. S. Dresselhaus, J. Phys. Chem. Solids **32**, 3 (1971).

[2]N. B. Brandt, E. A. Svistova, and M. V. Semenov, Zh. Eksp. Teor. Fiz. **59**, 434 (1970) [Sov. Phys. JETP **32**, 238 (1971)].

[3]N. B. Brandt, R. Hermann, G. I. Golysheva, L. I. Devyatkova, D. Kusnik, W. Kraak, and Ya. G. Ponomarev, Zh. Eksp. Teor. Fiz. **83**, 2152 (1982) [Sov. Phys. JETP **56**, 1247 (1982)]; G. A. Mironova, M. V. Sudakova, and Ya. G. Ponomarev, Fiz. Tverd. Tela (Leningrad) **22**, 3628 (1980) [Sov. Phys. Solid State **22**, 2124 (1980)].

[4]E. R. Youngdale, J. R. Meyer, C. A. Hofmann, F. J. Bartoli, D. L. Partin, C. M. Thrush, J. P. Heremans, Appl. Phys. Lett. **57**, 336 (1990); in *The Physics of Semiconductors,* Proceedings of the 20th International Conference on the Physics of Semiconductors, edited by E. M. Anastassakis and J. D. Joannopoulos (World Scientific, Singapore, 1990); Appl. Phys. Lett. **59**, 756 (1991); J. Cryst. Growth **111**, 693 (1991).

[5]Y. F. Ogrin, V. N. Lutskii, and M. I. Elinson, Pis'ma Zh. Eksp. Teor. Fiz. **3**, 114 (1966) [JETP Lett. **3**, 71 (1966)].

[6]V. S. Edel'man, Usp. Fiz. Nauk. **123**, 257 (1977) [Sov. Phys. Usp. **20**, 819 (1977)].

[7]R. N. Brown, J. G. Mavroides, and B. Lax, Phys. Rev. **129**, 2055 (1963).

[8]The group-V semimetals crystallize with $\bar{3}m$ symmetry, having one trigonal axis, and three bisectrix and three binary axes. To illustrate the similarlity between Bi and the closely related lead-chalcogenide narrow-gap semiconductors, rhombohedral Bi can be viewed as a distorted cubic crystal, with its trigonal axis along the cubic $\langle 111 \rangle$ direction, its bisectrix axis along a cubic $\langle 11\bar{2} \rangle$ direction, and its binary axis along a cubic $\langle 1\bar{1}0 \rangle$ direction. The four L-point ellipsoids of the Fermi surface of, for instance, PbTe, become in Bi three L-point electron ellipsoids and one T-point hole ellipsoid aligned with the trigonal axis.

[9]J. Heremans and O. P. Hansen, J. Phys. C **12**, 3483 (1976).

[10]M. P. Vecchi and M. S. Dresselhaus, Phys. Rev. B **10**, 771 (1974).

[11]R. J. Dinger and A. W. Lawson, Phys. Rev. B **12**, 5215 (1973).

[12]V. S. Edel'man and M. S. Khaikin, Zh. Eksp. Teor. Fiz. **49**, 107 (1965) [Sov. Phys. JETP **22**, 77 (1966)].

[13]M. S. Maltz and M. S. Dresselhaus, Phys. Rev. B **2**, 2877 (1970).

[14]M. P. Vecchi, J. R. Pereira, and M. S. Dresselhaus, Phys. Rev. B **14**, 298 (1976).

[15]J. Heremans and J.-P. Michenaud, J. Phys. C **18**, 6033 (1985).

[16]D. L. Partin, J. Heremans, D. T. Morelli, C. M. Thrush, C. H. Olk, and T. A. Perry, Phys. Rev. B **38**, 3818 (1988).

[17]D. L. Partin, C. M. Thrush, J. Heremans, D. T. Morelli, C. M. Thrush, and C. H. Olk, J. Vac. Sci. Technol. B **7**, 348 (1989).

[18]J. Heremans, D. T. Morelli, D. L. Partin, C. H. Olk, C. H. Thrush, and T. A. Perry, Phys. Rev. B **38**, 10 280 (1988).

[19]D. T. Morelli, D. L. Partin, and J. Heremans, Semicond. Sci. Technol. **5**, S257 (1990).

[20]A. L. Jain, Phys. Rev. **114**, 1518 (1959).